Applied Catalysis B: Environmental 84 (2008) 699–705

Contents lists available at ScienceDirect

Applied Catalysis B: Environmental

journal homepage: www.elsevier.com/locate/apcatb

Sn^{IV}-containing layered double hydroxides as precursors for nano-sized ZnO/SnO_2 photocatalysts

E.M. Seftel [a,b,*], E. Popovici [a], M. Mertens [c], E.A. Stefaniak [d,e], R. Van Grieken [d], P. Cool [b], E.F. Vansant [b]

[a] Department of Physical and Theoretical Chemistry and Materials Chemistry, "Al. I. Cuza" University of Iasi, Bvd. Carol I, No 11, 700506, Romania
[b] Laboratory of Adsorption and Catalysis, Department of Chemistry, University of Antwerpen (CDE), Universiteitsplein 1, 2610 Wilrjik, Antwerpen, Belgium
[c] VITO Flemish Institute for Technological Research, Boeretang 200, B-2400, Belgium
[d] Environmental Analysis Laboratory, Department of Chemistry, University of Antwerp, Universiteitsplein 1, Antwerp 2610, Belgium
[e] Department of Chemistry, Catholic University of Lublin, Al. Kraśnicka 102, Lublin 20-718, Poland

ARTICLE INFO

Article history:
Received 28 February 2008
Received in revised form 28 May 2008
Accepted 3 June 2008
Available online 18 June 2008

Keywords:
Sn^{4+} containing LDHs
ZnO/SnO_2 systems
Charge separation
Photocatalysis
Methyl orange

ABSTRACT

Sn^{4+}-containing LDH was prepared using the co-precipitation method at constant pH, and characterized using X-ray diffraction, UV–vis diffuse reflectance spectroscopy and TG/DTG methods. The obtained product was further exposed to different thermal treatments in order to obtain nano-sized coupled ZnO/SnO_2 systems with enhanced photocatalytic performances than the ones obtained by mixing the two semiconductor oxides. The formation of a well-defined ZnO/SnO_2 system and the crystallite size, fully investigated using XRD, micro-Raman scattering and UV–vis DR techniques, were found to be influenced by the nature of the precursors and the calcination temperature. The photocatalytic activity of the ZnO/SnO_2 systems, evaluated for the photodegradation of methyl orange (MO) dye, was studied as a function of the initial pH, catalyst loading and the calcination temperature. The metal dispersion supplied by layered structures proved to be an advantage when preparing coupled ZnO/SnO_2 systems, the photocatalytic activity being ~2.3 times higher comparing with the physical mixtures performances. The maximum photocatalytic activity of the coupled ZnO/SnO_2 system having a layered precursor was observed when using neutral pH, at a catalyst loading of 1 g/L calcined at 600 °C for 4 h.

1. Introduction

Layered double hydroxides (LDHs) having hydrotalcite-like structures are a family of lamellar solids which received a considerable interest in recent years due to their potential application in numerous domains, such as in green chemistry, catalysis, as precursors for catalysts, etc. [1,2]. This is due to the possibility to obtain mixed metal oxides at the atomic level, rather than at a particle level throughout thermal decomposition of the layered precursor.

These materials originate from the isomorphous substitution of divalent cations, such as Mg^{2+}, by trivalent cations, like Al^{3+}, in a brucite-like structure. Both Mg^{2+} and Al^{3+} can be replaced by other di- or trivalent cations giving rise to a wide variety of LDHs having the general formula $[M_{1-x}^{2+}M_x^{3+}(OH)_2]\cdot(A_{x/n}^{n-})\cdot mH_2O$, where M^{2+} and M^{3+} are the divalent and trivalent cations, respectively, and A^{n-} the interlayer anions [2]. Lately, it was shown that tetravalent cations such as Ti^{4+} [3,4], Zr^{4+} [5] and Sn^{4+} [6,7] could also be incorporated in the brucite-like LDH layer.

Photocatalytic purification of waste waters by irradiated semiconductor particles has proven to be a very effective process, which leads to complete mineralization of pollutants [8–10]. When the semiconductor particles absorb a photon of energy equal to or greater than the band gap energy width, an electron is promoted from the valence band to the conduction band leaving behind an electron vacancy or hole in the valence band. The hole may react with surface-bound H_2O or HO^- and produce the $HO^\bullet$ radicals which are widely accepted to be the primary oxidizing species in the photocatalytic processes [11]. The photocatalytic activity strongly depends on the energy of the electron–hole pairs produced as well as their separation. A wider separation of the electrons and holes enhances the photocatalytic activity by reducing the recombination. A good charge separation may be achieved by coupling two semiconductor particles having different band positions. The layered structures can supply a good metal dispersion and may represent an advantage for subsequent applications.

* Corresponding author at: Laboratory of Adsorption and Catalysis, Department of Chemistry, University of Antwerpen (CDE), Universiteitsplein 1, 2610 Wilrjik, Antwerpen, Belgium. Tel.: +32 3 820 23 53; fax: +32 3 820 23 74.
E-mail address: seftel_elena@yahoo.com (E.M. Seftel).

0926-3373/$ – see front matter © 2008 Elsevier B.V. All rights reserved.
doi:10.1016/j.apcatb.2008.06.006

The present study focuses on the possibility of total replacement of the trivalent Al^{3+} cations by the tetravalent Sn^{4+} cations in a Zn/Al-LDH, and to investigate either the Sn^{4+} cations could be incorporated within the brucite-like sheets or segregated in different phases. Furthermore, the as-synthesized Zn/Sn-LDH was exposed to a thermal treatment in order to investigate the possibility to obtain a nanosized coupled ZnO/SnO_2 with potential applications in photocatalytic processes.

2. Experimental

2.1. Samples preparation

$ZnCl_2$ (Fluka, >98%), $AlCl_3{\cdot}6H_2O$ (Fluka, >99%), $SnCl_4{\cdot}5H_2O$ (Acros, 98+%), NaOH (Acros, 99.5%) and Na_2CO_3 (Jansen Chemica) were used as received.

ZnAl- and ZnSn-LDHs with the cationic Zn^{2+}/Al^{3+} and Zn^{2+}/Sn^{4+} ratio of 3 were prepared by the co-precipitation method at constant pH [2]. The synthesis was carried out by the slow addition of a mixed metal chlorides solution (1 M in total) to a Na_2CO_3 (2×10^{-3} M) solution under magnetic stirring. During the synthesis the pH value was kept constant at 7.5 by adding suitable amounts of 2 M NaOH solution. The resulting precipitates were aged at room temperature for 24 h under magnetic stirring, then filtered, washed several times with distilled water and dried at room temperature. These samples were denoted as ZnAl-3 and ZnSn-3, respectively. Part of the as-synthesized samples were calcined at 500 and 700 °C in a Lenton furnace for 4 h (1° min^{-1}) and denoted as CZnAl-3-T and CZnSn-3-T, where T stands for the calcination temperature.

ZnO and SnO_2 as reference samples were prepared following the same procedure, but the starting solutions contained only $ZnCl_2$ (1 M) or $SnCl_4{\cdot}5H_2O$ (1 M), respectively.

To compare both structural and photocatalytic features of the obtained coupled ZnO/SnO_2 nano-sized systems, three physical mixtures were obtained by grinding appropriate amounts of as-synthesized ZnO and SnO_2 followed by calcination at 500 °C, 600 °C and 700 °C for 4 h (1° min^{-1}).

2.2. Photocatalytic tests

The photocatalytic activity of both ZnSn-3 and physical mixture samples calcined at different temperatures were tested for the photodegradation of methyl-orange in aqueous solution. Appropriate amounts catalyst were added to 25 mL methyl-orange (MO) solution (4×10^{-5} M) in a plastic flask and stirred for 30 min without UV-irradiation in order to establish the adsorption–desorption equilibrium between the dye and the surface of the catalyst. After 30 min, the suspension was irradiated with UV-light for 80 min. The UV-light source was a 100 W Hg lamp (Sylvania Par 38, 365 nm). During the irradiation, at intervals of 10 min, samples (5 mL) of the suspension were collected, centrifuged and analyzed at 463 nm using water as reference with a Thermo-electron evolution 500 UV–vis spectrometer. Immediately after the analysis the sample was placed back to the solution.

2.3. Characterization techniques

The final composition of the as-synthesized samples was determined by electron probe micro analysis measurements (EPMA). X-ray diffractions were recorded on a PANalytical X'Pert PRO MPD diffractometer with filtered Cu Kα radiation; measurements were done in the 2θ mode using a bracket sample holder with a scanning speed of 0.04°/4 s continuous mode. Thermoanalytical measurements were performed on a Mettler Toledo TGA/SDTA851^e thermobalance. Samples were heated at a heating rate of 5 °C/min under O_2 flow. UV–vis-DR spectra were obtained at room temperature on a NICOLET EVOLUTION 500 UV–vis Spectrometer, with a diffuse reflectance accessory using KBr standard white as reflectance. Raman spectra were recorded with a Renishaw InVia micro-Raman spectrometer coupled with a Leica microscope and equipped with Peltier cooled CCD detector. Excitation was provided by 785 nm laser (300 mW source power). Samples were scanned using a synchroscan mode from 100 cm^{-1} to 2000 cm^{-1} at a spectral resolution of about 2 cm^{-1}. The acquisition time for each scan as well as the number of accumulations varied in order to provide a better signal-to-noise ratio. Spectra were obtained using 50× or 20× magnification objectives. Calibration was done for the 520.5 cm^{-1} line of silicon.

3. Results and discussion

3.1. Composition and structure

Table 1 summarizes the chemical compositions and structural properties of the as-synthesized samples, while their XRD patterns are shown in Fig. 1.

The chemical analyses results, referred to the total amount of metal ions in the obtained solids, is close to the ones in the starting solutions, indicating that the reaction of precipitation was complete; however, this is not an indication of the effective incorporation of Sn^{4+} cations into the brucite-like sheets of the obtained LDH.

The Zn_3Sn-LDH pattern exhibits the typical (0 0 3) reflection of layered structure and the interlayer spacing indicates the presence of carbonate anions in the interlayer region. The decrease of the interlayer spacing of ZnSn-3, comparing to the ZnAl-3 sample, and therefore, the decrease of the c unit cell parameter, indicates that a part of tin is incorporated within the brucite-like sheets. This observation may be attributed to the increase of the layer charge density and a consequent decrease of the interlayer distance, as observed by Velu et al. [6]. Moreover, the increased value of the a parameter in the Sn-containing LDH indicates the partial incorporation of the tin cations within the brucite-like sheets, as the ionic radius of Sn^{4+} (0.69 Å) is higher than for the Al^{3+} (0.50 Å). In addition to the LDH phase, a zinc hydroxo stannate ($ZnSn(OH)_6$) phase is noticed [12]. In the initial stage of the synthesis reaction, the LDHs crystals are formed together with a $ZnSn(OH)_6$ phase. The complex $Sn(OH)_6^{2-}$ is formed in the synthesis mixture most likely due to the excess amount of NaOH. Consequently, less tetravalent cations are available to form the Zn/Sn-LDH structure leaving an excess of Zn^{2+} cations in the reaction mixture. These Zn^{2+} cations,

Table 1
Chemical compositions and structural properties of the as-synthesized samples

Sample	ZnAl-3	ZnSn-3
[a]Zn/Al/Sn molar ratio	3.0/0.9/0.0	3.0/0.0/0.81
XRD phase observed	LDH	LDH + ZHS
a (Å)	3.06	3.08
c (Å)	23.6	23.3
$d_{0\,0\,3}$ (Å)	7.87	7.77
[b]The thickness of the interlayer gallery (Å)	3.07	2.97

LDH: layered double hydroxide phase; ZHS: zinc hydroxo stannate [$ZnSn(OH)_6$] phase. $a = 2d_{1\,1\,0}$ and $c = 3d_{0\,0\,3}$ of LDH phase.
[a] Calculated from the EPMA results.
[b] The difference between $d_{0\,0\,3}$ and 4.8 Å (the thickness of the brucite-like sheet) [1].

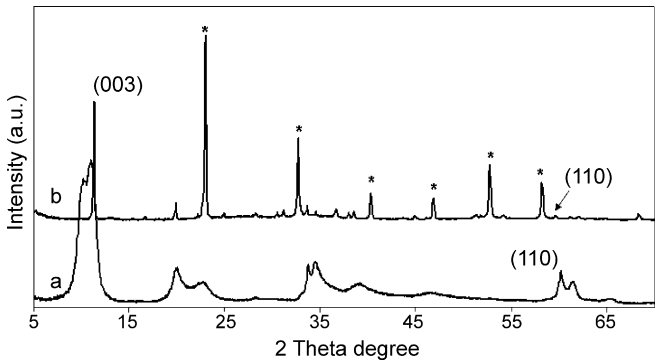

Fig. 1. The XRD patterns of (a) ZnAl-3 and (b) ZnSn-3 sample; (*) $ZnSn(OH)_6$ phase.

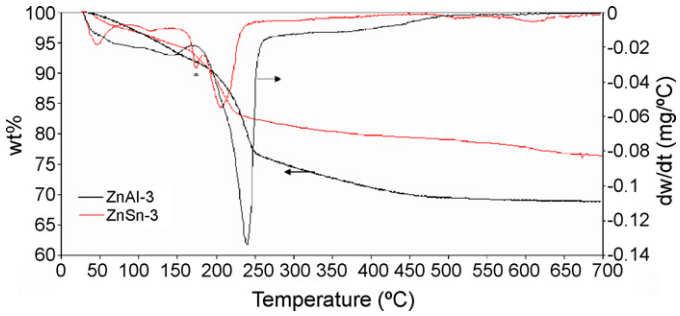

Fig. 3. The TG/DTG curves of the ZnSn-3 and ZnAl-3 samples; (*) dehydroxylation of the ZHS phase.

in the presence of NaOH, will form the $Zn(OH)_4^{2-}$ complex, which together with the $Sn(OH)_6^{2-}$ complex, will act as nuclei for the formation of the $ZnSn(OH)_6$ phase:

$$Zn^{2+} + Sn^{4+} + HO^- \longrightarrow (Zn,Sn)(OH)_2 + Zn(OH)_4^{2-} + Sn(OH)_6^{2-}$$

$$\text{LDH phase} \qquad ZnSn(OH)_6 + 4\,HO^-$$

Fig. 2 displays the UV–vis DR spectra of the as-synthesized samples and confirms the presence of both tetra-coordinated as segregated tin species as well as hexa-coordinated tin species within the brucite-like sheets. As expected, the sample without Sn^{4+} exhibits a very low intensity absorption spectrum. After incorporation of tetravalent cations, two absorption bands with maxima at 238 nm and ~250 nm are observed. The first absorption at 238 nm can be assigned to $O^{2-} \rightarrow Sn^{4+}$ charge transfer transition of the Sn ions in a tetrahedral environment. The broad absorption band centered at ~250 nm can be assigned to the Sn^{4+} cations in an octahedral environment [13,14].

The thermal stability of the Sn-containing sample was studied using TG/DTG method. Fig. 3 displays the TG/DTG curves of ZnSn-3 and ZnAl-3 samples. The first two endothermic transitions observed at 49 and 121 °C observed in the DTG curve of the ZnSn-3 sample correspond to the water loss from the external surface (12.12 wt%) and from the interlayer gallery (15.2 wt%), respectively. The lamellar structure decreases in stability and collapses at ~210 °C when the decomposition of the carbonate anions and the dehydroxylation of the brucite-like sheets occurs (ca. 50.83 wt%). An endothermic peak at 175 °C is observed which, correlated with the XRD observations, may be attributed to the dehydroxylation of the zinc hydroxo stannate (ZHS) phase with a concomitant loss of 9.72 wt% [6]. Two additional endothermic transitions are observed at higher temperatures, in the range between 500 °C and 700 °C, which can be probably attributed to the conversion into the ZnO/SnO_2 lattice. These transformations were also confirmed by XRD and micro-Raman measurements (Figs. 4 and 5).

The XRD patterns of the tin containing solid calcined at different temperatures for 4 h are shown in Fig. 4. The XRD patterns show the presence of two phases: ZnO with a wurtzite type structure [15,16] and SnO_2 with a tetragonal rutile structure [17]. The heat treatment at 500 °C for 4 h leads to the rapid crystallization of the ZnO phase. The crystallization and the growth of the SnO_2 phase can be correlated with the decomposition of the $ZnSn(OH)_6$ phase. The diffraction peaks attributed to $ZnSn(OH)_6$ phase thoroughly disappeared. Therefore, the SnO_2 crystallization process is accomplished by eliminating the zinc hydroxo stannate phase, obtaining very small crystalline grains as well as amorphous phase. Increasing the temperature up to 700 °C leads to the formation of a well crystallized coupled ZnO/SnO_2 system and the process can be illustrated as follows:

$$(Zn,Sn)(OH)_2 + ZnSn(OH)_6 \xrightarrow{\sim 175^\circ C} (Zn,Sn)(OH)_2 + (ZnO/SnO_2) + 3H_2O\uparrow \xrightarrow{\sim 210^\circ C}$$

$$\xrightarrow{\sim 210^\circ C} (Zn,Sn)O^{2-} + (ZnO/SnO_2) + H_2O\uparrow \xrightarrow{500\text{-}700^\circ C} ZnO/SnO_2$$

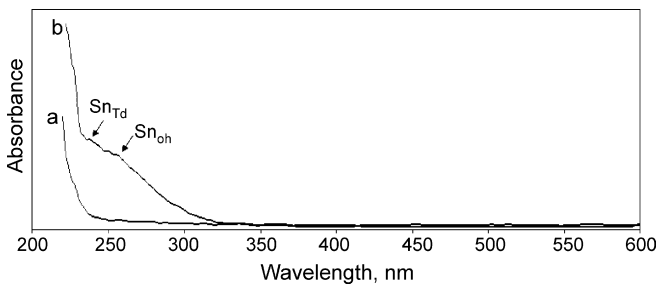

Fig. 2. The UV–vis DR spectra of (a) ZnAl-3 and (b) ZnSn-3 sample.

The crystallite size of the observed ZnO and SnO_2 phases were calculated and the results are listed in Table 2. The crystallite sizes were estimated by using the Scherrer equation [18] and selecting the crystal planes of (1 0 1) and (1 1 0) for ZnO and SnO_2, respectively. The data showed that the growth of the crystals in the ZnO/SnO_2 system is sensitive to the calcination temperature (Table 2). As previously reported [19], the growth of the ZnO nanoparticles was found to be inhibited by the presence of SnO_2 phase when the heat treatment increases up to 600 °C and 700 °C.

The formation of the coupled ZnO/SnO_2 system as the calcination temperature increased form 500 °C to 700 °C was investigated using micro-Raman scattering. ZnO with a wurtzite-type structure belongs to the C_{6v} space group or 6 mm symmetry with the photon modes E_2 (high), A_1 (TO-transversal acoustic mode and LO-longitudinal optical components) and E_1 (TO and LO) [20,21]. The tetragonal rutile SnO_2 belongs to the $D14_{4h}$ space group with the optical modes A_{1g}, B_{1g}, B_{2g} and E_g [22,23]. Fig. 5 displays the micro-Raman spectra of the obtained solids. The peaks centered at 330, 380

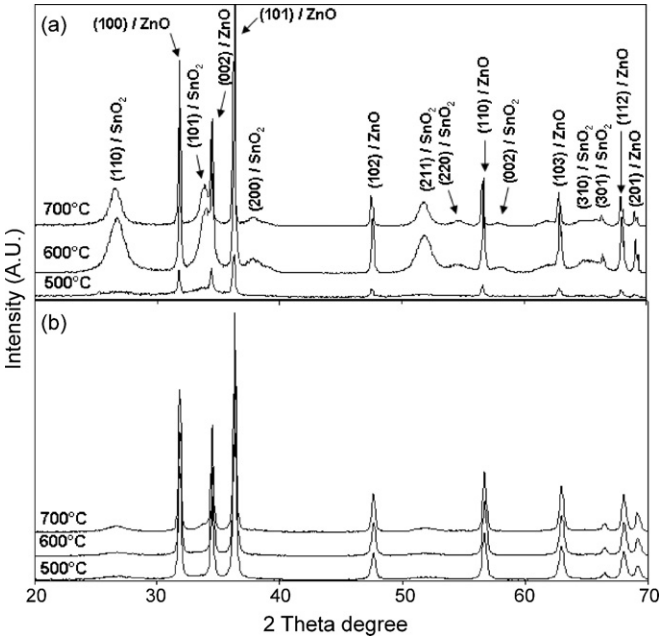

Fig. 4. The XRD patterns of (a) CZnSn-3 and (b) physical mixtures (3/1) samples calcined at different temperatures for 4 h.

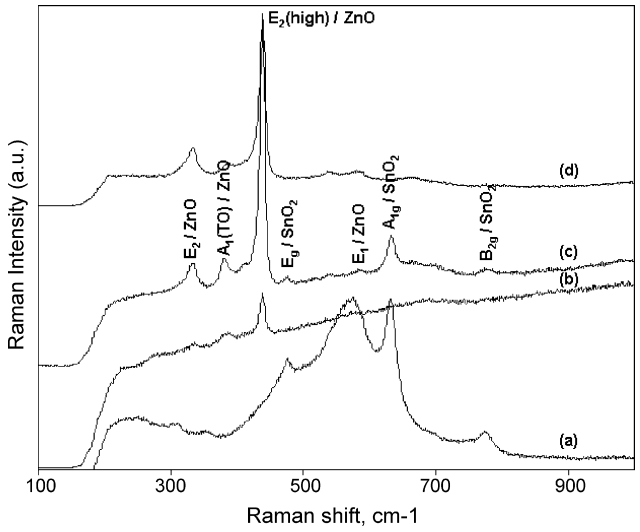

Fig. 5. The micro-Raman spectra of (a) SnO_2, (b) CZnSn-3-500 °C, (c) CZnSn-3-700 °C and (d) ZnO samples.

and 438 cm^{-1} observed in the Raman spectrum of the ZnSn-3-500 °C can be attributed to the second order E_2 mode, A_1 (TO) and E_2 (high) modes of ZnO with a wurtzite-type structure. The XRD patterns showed that at 500 °C very small SnO_2 nanoparticles are formed (2.7 nm). The B_{2g} mode has been observed to disappear in the Raman spectra in the case of very small SnO_2 nanoparticles (<4 nm) [24]. Therefore, the first endothermic transition at higher temperatures (~500 °C) observed in the DTG curve may be attributed to the conversion mainly into a ZnO lattice. Additional peaks are observed in the Raman spectrum of the tin-containing sample when the calcination temperature increased up to 700 °C. The peaks centered at 632 and 775 cm^{-1} may me assigned to the A_{1g} and B_{2g}, respectively, and are related to the expansion and contraction vibration modes of Sn–O bonds in the rutile structure of SnO_2. The peak observed at 472 cm^{-1} may be attributed to the E_g mode of the SnO_2 phase. The appearance of the B_{2g} mode may be correlated with the growth of the SnO_2 nanoparticles when the calcination temperature increased, which is in agreement with the XRD data (Table 2).

Fig. 6 displays the UV–vis diffuse reflectance spectra for the Sn-containing LDH and for the physical mixtures ZnO/SnO_2 calcined at different temperatures for 4 h. The wavelength of the absorption edges were determined by extrapolating the sharply rising and horizontal portions of the UV–vis curves and defining the edges as the wavelengths of the intersection [25]. Literature data report that the n-type semiconductor ZnO has a band gap energy of 3.2 eV and the SnO_2 shows not only a direct band gap energy of 3.5–3.9 eV but also an indirect band gap energy of ~2.6 eV [8,25]. The calculated band gap energy of the pure ZnO calcined at 500 °C, 600 °C and 700 °C for 4 h are 3.16 eV, 3.17 eV and 3.17 eV, respectively, indicating that the band gap energy is not influenced by the calcination temperature, which is in agreement with the literature reports for the ZnO nanoparticles [8]. The absorption curves of the SnO_2 samples calcined at 500 °C, 600 °C and 700 °C for 4 h (Fig. 6d) display significant tail. The calculated band gap values indicated an indirect transition which is increasing with the increase of the temperature (*e.g.* 2.92 eV, 2.98 eV and 3.1 eV, respectively). The coupled ZnO/SnO_2 photocatalysts obtained from both physical mixtures and LDH precursor are a mixture of ZnO and SnO_2, as demonstrated in Fig. 4. Therefore, the UV–vis spectra should show the contribution of both phases. One-edge absorption is observed in the case of the physical mixtures calcined at 500 °C, 600 °C and 700 °C for 4 h (Fig. 6b) representing mainly the contribution of the ZnO nanoparticles indicating again that the heat treatment for 4 h is not sufficient for the formation of well crystallized SnO_2 grains and, therefore, a good ZnO/SnO_2 coupled system.

By contrast, the ZnO/SnO_2 systems having a LDH precursor, calcined at 500 °C, 600 °C and 700 °C for 4 h displayed a two-edge absorption showing the contribution of both ZnO and SnO_2 phases.

3.2. Photocatalytic experiments

The decolorization of a dye is initiated by the photoexcitation of the semiconductor system followed by the formation of the electron/hole pairs on the surface of the catalyst:

$$(ZnO/SnO_2) + h\nu \rightarrow (ZnO/SnO_2)(e^-_{CB} + h^+_{VB})$$

Table 2
Dependence of the crystallite size on the heat-treatment conditions

ZnSn-3			
Heat-treatment conditions	500 °C	600 °C	700 °C
Phase/crystallite size[a] (nm)	ZnO/29.3 SnO_2/amorphous; 2.7	ZnO/31 SnO_2/5.3	ZnO/37.2 SnO_2/8.1
Physical mixtures (3/1)			
Heat-treatment conditions	500 °C	600 °C	700 °C
Phase/crystallite size[a] (nm)	ZnO/31.7 SnO_2/amorphous; 6.9	ZnO/34.6 SnO_2/amorphous; 7.43	ZnO/38.1 SnO_2/amorphous; 10.3

[a] Calculated using the Scherrer equation [18].

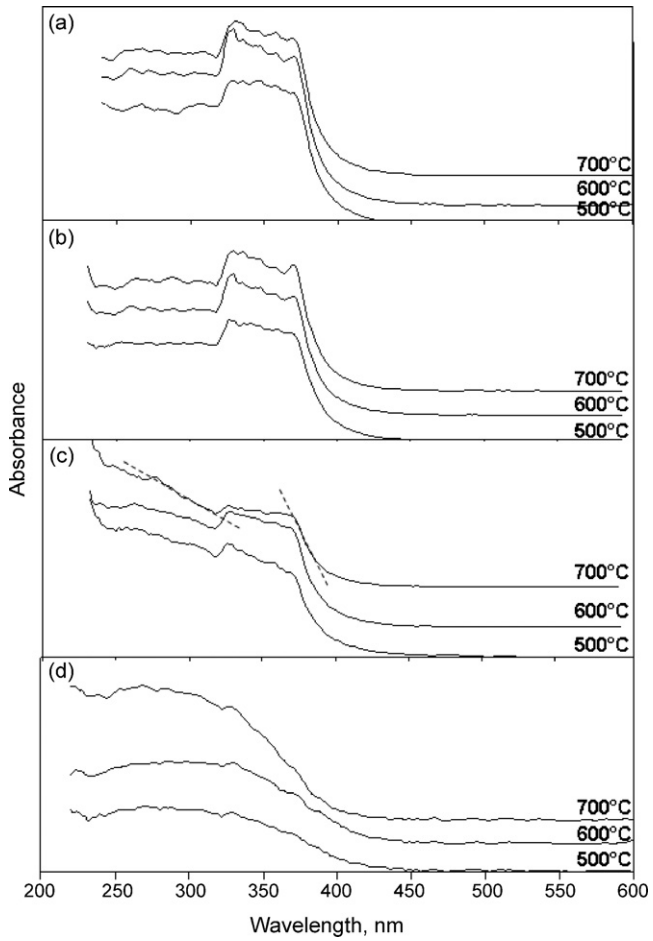

Fig. 6. The UV–vis DR spectra of (a) ZnO, (b) physical mixtures (3/1), (c) ZnSn-3 and (d) SnO_2 samples calcined for 4 h at different temperatures.

The hydroxide radical ($HO^{\bullet}$), responsible for the dye degradation, is formed by the decomposition of the water or by reaction of the holes with HO^{-}:

$$h_{VB}^{+} + H_2O \rightarrow H^{+} + HO^{\bullet}$$

$$h_{VB}^{+} + HO^{-} \rightarrow HO^{\bullet}$$

$$HO^{\bullet} + \text{dye} \rightarrow \text{degradationofthedye}$$

An efficient photocatalytic process requires highly crystalline semiconductors to minimize the electron/hole recombination. In the present experimental conditions, this requirement is only satisfied by the photocatalytic system having a layered precursor. The SnO_2, with a conduction band lower than that of ZnO, can act as a sink for the photogenerated electrons and the holes may be trapped within the ZnO nanoparticle. The intimate contact created facilitates the electron/hole transfer between the two semiconductors increasing the efficiency of the charge separation, the entire system showing stronger photocatalytic activity (Fig. 7).

The photocatalytic activity was evaluated for the degradation of methyl-orange dye in aqueous solution as a function of catalyst dose (0.1–2.0 g/L), initial pH (2–10), and calcination temperature (500–700 °C). Blank experiments were carried out without UV light or catalyst to verify that the color removal of MO was indeed due to the photocatalytic process (Fig. 8). The experiment conducted in the absence of the photocatalyst but under UV light demonstrated that the MO could not be degraded. The same result

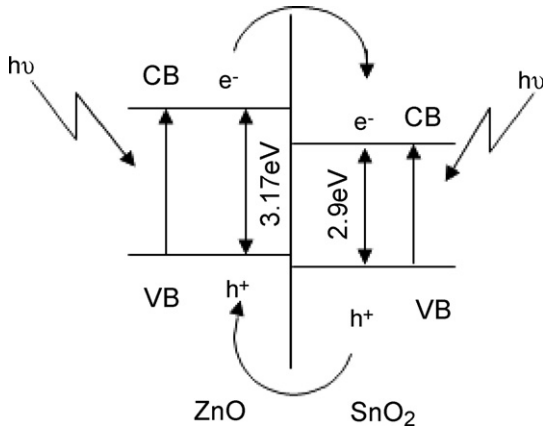

Fig. 7. The schematic illustration of the electron transfer and the energy level diagram indicating the band positions of the ZnO and SnO_2 in the photocatalytic system.

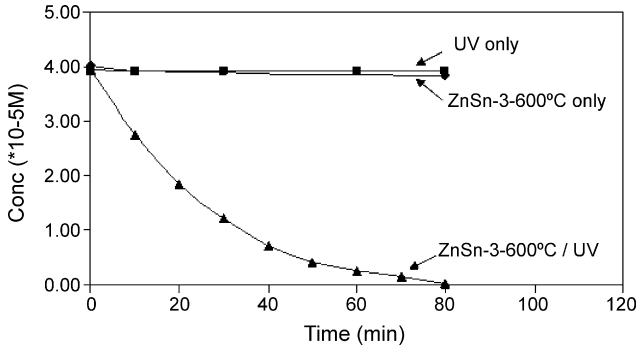

Fig. 8. Degradation kinetics of MO in the presence UV light only, ZnSn-3-600 °C with and without UV light (catalyst: 1 g/L; MO: 4×10^{-5} M, pH 6).

was obtained when the experiment was conducted in the presence of the photocatalyst but without UV irradiation.

3.2.1. Effect of catalyst dose

To determine the optimal catalyst dose for the photocatalytic degradation of MO, several experiments were conducted by varying the catalyst loading from 0.1 g/L to 2 g/L at a constant dye concentration (4×10^{-5} M), initial pH (~6) and irradiation time (80 min). Fig. 9 illustrates the effect of the catalyst dose on the decolorization efficiency of MO dye. A maximum is observed when using a catalyst dose of 1 g/L (99%), at higher loadings the efficiency of decolorization remaining almost at a constant value (94%). This result is similar to the results reported in the literature for the optimum catalyst loading [26,27] and can be explained on the basis of the total active sites on the catalyst surface. When increasing the catalyst dose until an optimal loading is achieved, a higher catalyst

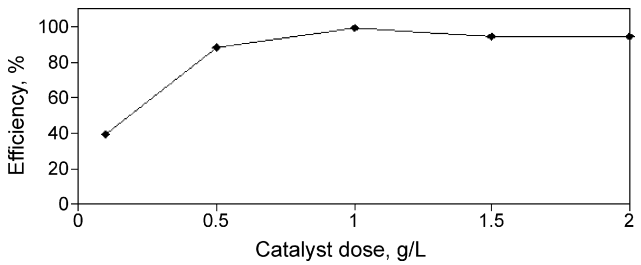

Fig. 9. The effect of the catalyst dose on the decolorization efficiency of MO (pH 6, MO: 4×10^{-5} M).

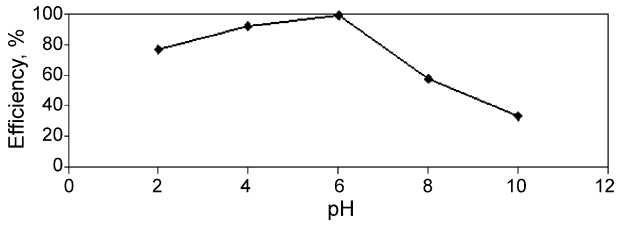

Fig. 10. The pH dependence of the photocatalytic efficiency of the ZnSn-3-600 °C sample (catalyst: 1 g/L; MO: 4×10^{-5} M).

dosage causes higher color removal efficiency due to the creation of a higher number of active species. More catalyst will lead to the formation of more HO• radicals, which are widely accepted as principal oxidizing species responsible for the photodegradation process [11]. The increase of the catalyst dosage above the optimal limit leads to the increase of the turbidity of the suspension decreasing the penetration of the UV light and, as a consequence, the decrease of the HO• radicals formation. Therefore, a catalyst dose of 1 g/L was fixed for further studies.

3.2.2. Effect of initial pH

To study the effect of the pH on the photodegradation efficiency, experiments were carried out at different initial pH values, ranging between 2 and 10, at constant catalyst dose (1 g/L) and at a fixed reaction time (80 min) and dye concentration (4×10^{-5} M). The pH was adjusted in acid and alkaline media using HCl (1 M) and NaOH (1 M), respectively. Fig. 10 illustrates the removal efficiency of MO as a function of the initial pH. The experimental data showed that the removal efficiency of MO increases with the increase of pH reaching a maximum of degradation at pH 6 and, then, decreases as the pH increase. These results can be explained taking into account the acid–base property of the metal oxides surface in water [16]. At low pH value, the MO is negatively charged ($pK_a = 3.8$), whereas the catalyst is positively charged below pH ~9. The photocatalytic activity can thus be explained in terms of electrostatic interactions between the catalyst surface and the dye. Moreover, the photocatalytic system is not chemically stable in very acidic media leading to a decreased value of the decolorization degree (it should be noted that we observed the partial dissolution of the photocatalytic system at very low pH value). At high pH values, a decrease of the photocatalytic activity is observed and is consistent with the establishment of coulombic repulsion between the anions and the highly negative charged catalyst surface. The increase of the pH might also cause a cathodic displacement of the valence band position of ZnO and SnO_2 in the ZnSn-3-600 °C photocatalyst and results in the weakening of the oxidation ability of the holes [19,28].

3.2.3. Effect of the calcination temperature

The effect of the calcination temperature on the photocatalytic activity of the ZnSn-3 sample is shown in Fig. 11. It can be seen that the photocatalytic activity increases with the increase of the calcination temperature up to 600 °C, and no significant difference among the catalysts calcined at 600 °C and 700 °C is observed.

As mentioned above, the heat treatment at 500 °C for 4 h leads to the formation of a well crystallized ZnO phase together with SnO_2 mostly as amorphous phase. On the other hand, we can observe that the photocatalytic activity increases when the sample was treated at 600 °C, total degradation being achieved in 80 min, above this temperature the photocatalytic activity remaining almost constant. Taking onto account the XRD and UV–vis DR data, the increase of the photocatalytic activity observed for the ZnSn-3 sample calcined at 600 °C for 4 h may be attributed to the formation of a well crystallized ZnO/SnO_2 system, comparing with the one obtained from the physical mixture of the two

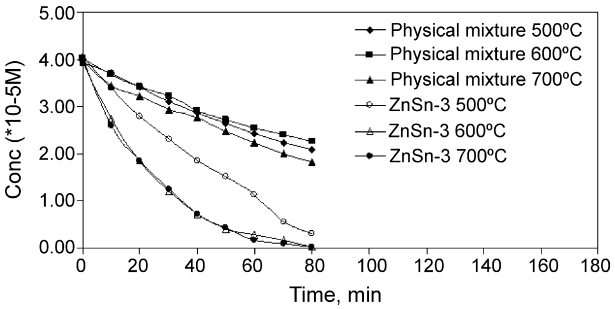

Fig. 11. The effect of the calcination temperature (for 4 h) on the photocatalytic activity of the ZnSn-3 and physical mixture samples (catalyst: 1 g/L; pH 6; MO: 4×10^{-5} M).

semiconductor oxides. No other phases were observed in the XRD patterns which might reduce the photocatalytic activity when the samples are treated at higher temperatures, *e.g.* Zn_2SnO_4 with low photocatalytic activity, showing that the heat treatment for 4 h at the specified temperatures is not sufficient for the solid state reaction between the ZnO and SnO_2 phases. The presence of Sn^{4+} cations hinders the formation of the spinel-like phase in temperature, as observed by Intissar et al. [29], and more drastic conditions (*e.g.* higher temperature and/or time) are needed by solid state reaction to obtain the spinel-like phase, showing that the metal dispersion supplied by the double layered structure is an advantage for subsequent applications. Moreover, an intimate contact had been created between the two semiconductor oxides which had a direct influence on the separation of the electrons and holes enhancing the photocatalytic activity by reducing the recombination.

4. Conclusions

ZnAl- and ZnSn-layered double hydroxides were prepared by the co-precipitation method at constant pH. The XRD, UV–vis DR and TG/DTG methods revealed that an additional zinc hydroxo stannate phase is formed. The obtained product was exposed to a thermal treatment in order to obtain a nano-sized coupled ZnO/SnO_2 system with higher photocatalytic activity than the ones obtained by mixing the two semiconductor oxides. The data showed that the heat treatment for 4 h of the ZnSn-3 sample was sufficient for the formation of a well-defined ZnO/SnO_2 system. The efficiency of the photodegradation increased when the initial pH has a neutral value and with the increase of the catalyst dosage up to an optimum loading. The experimental results indicated that the degradation of the MO dye is facilitated in the presence of the ZnO/SnO_2 systems having a layered precursor, showing that the metal dispersion supplied by these structures is an advantage for subsequent applications.

Acknowledgments

This study was supported by the NoE project "Inside Pores" and the GOA project funded by the Special Fund for Research of the University of Antwerp. This work is also part of the CEEX No. 1/S1/2005 project.

References

[1] P.S. Braterman, Z.P. Xu, F. Yarberry, in: S.M. Auerbache, K.A. Carrado, P.K. Dutta (Eds.), Handbook of Layered Materials, Marcel Dekker, Inc., New York, 2004, p. 373.
[2] F. Cavani, F. Trifiro, A. Vaccari, Catal. Today 11 (1991) 201.
[3] E.M. Seftel, E. Popovici, M. Mertens, G. Van Tendeloo, P. Cool, E.F. Vansant, Micropor. Mesopor. Mater. 111 (2008) 12–17.

[4] O. Saber, H. Tagaya, J. Incl. Phenom. Macrocyclic Chem. 45 (2003) 109–116.
[5] C. Jiménez-Sanchidrián, J.M. Hidalgo, R. Llamas, J.R. Ruiz, Appl. Catal. A: Gen. 312 (2006) 86–94.
[6] S. Velu, K. Suzuki, T. Osaki, F. Ohashi, S. Tomura, Mater. Res. Bull. 34 (1999) 1707–1717.
[7] M.P. Kapoor, Y. Matsumura, Catal. Today 93–95 (2004) 287–291.
[8] C. Wang, X. Wang, B.Q. Xu, J. Zhao, B. Mai, P. Peng, G. Sheng, J. Fu, J. Photochem. Photobiol. A: Chem. 168 (2004) 47–52.
[9] S.K. Kansal, M. Singh, D. Sud, J. Hazard. Mater. 141 (2007) 581–590.
[10] K. Tennakone, J. Bandara, Appl. Catal. A: Gen. 208 (2001) 335–341.
[11] J. Nishio, M. Tokumura, H.T. Znad, Y. Kawase, J. Hazard. Mater. B138 (2006) 106–115.
[12] G. Cheng, K. Wu, P. Zhao, Y. Cheng, X. He, K. Huang, J. Cryst. Growth 309 (2007) 53–59.
[13] P. Shah, A.V. Ramaswamy, K. Lazar, V. Ramaswamy, Micropor. Mesopor. Mater. 100 (2007) 210–226.
[14] G. Luo, S. Yan, M. Qiao, K. Fan, Appl. Catal. A: Gen. 332 (2007) 79–88.
[15] R.E. Marotti, D.N. Guerra, C. Bello, G. Machado, E.A. Dalchiele, Sol. Energy Mater. Sol. Cells 82 (2004) 85–103.
[16] R. Comparelli, E. Fanizza, M.L. Curri, P.D. Cozzoli, G. Mascolo, A. Agostiano, Appl. Catal. B: Environ. 60 (2005) 1–11.
[17] M.R. Yang, S.Y. Chu, R.C. Chang, Sens. Actuators B 122 (2007) 269–273.
[18] Z. Chang, D.G. Evans, X. Duan, C. Vial, J. Ghabaja, V. Prevot, M. De Roy, C. Forano, J. Solid State Chem. 178 (2005) 2766.
[19] C. Wang, J. Zhao, X. Wang, B. Mai, G. Sheng, P. Peng, J. Fu, Appl. Catal. B: Environ. 39 (2002) 269–279.
[20] L. Shi, H. Shen, L. Jiang, X. Li, Mater. Lett. 61 (2007) 4735–4737.
[21] O. Lupan, L. Chow, G. Chai, B. Roldan, A. Naitabdi, A. Schulte, H. Heinrich, Mater. Sci. Eng. B 145 (2007) 57–66.
[22] S.K. Tripathy, T. Sahoo, I.H. Lee, Y.T. Yu, Mater. Lett. 61 (2007) 4690–4693.
[23] Y. Liu, F. Yang, X. Yang, Colloids Surf. A: Physicochem. Eng. Aspects 312 (2008) 219–225.
[24] P.L. Johnson, D. Teeters, Solid State Ionics 177 (2006) 2821–2825.
[25] C. Wang, B.Q. Xu, X. Wang, J. Zhao, J. Solid State Chem. 178 (2005) 3500–3506.
[26] N. Daneshvar, D. Salari, A.R. Khataee, J. Photochem. Photobiol. A: Chem. 157 (2003) 111–116.
[27] M.S.T. Gonclaves, A.M.F. Oliveira-Campose, M.J.R.P. Queiroz, Chemosphere 39 (1999) 781.
[28] I. Poulios, M. Kositzi, A. Kouras, J. Photochem. Photobiol. A: Chem. 115 (1998) 175–183.
[29] M. Initissar, F. Malherbe, V. Prévot, F. Leroux, J. Colloids Interface Sci. 299 (2006) 747–753.